Mangroves as a Source of Alkalinity and Dissolved Carbon to the Coastal Ocean: A Case Study from the Everglades National Park, Florida

Gloria M. S. Reithmaier[1], David T. Ho[2], Scott G. Johnston[1], Damien T. Maher[1]

[1]Southern Cross Geoscience, Southern Cross University, Lismore, New South Wales, Australia.

[2]Department of Oceanography, University of Hawaii at Manoa, Honolulu, Hawaii 96822, USA

Corresponding author: Gloria Reithmaier (g.reithmaier.10@student.scu.edu.au)

Key Points:

- Estuarine carbon dynamics were driven by carbon remineralization, carbonate dissolution and porewater inputs
- The mangrove-dominated estuary was a source of dissolved carbon and greenhouse gas emissions
- Dissolved inorganic carbon export was severalfold higher than carbon burial and should be therefore integrated in blue carbon budgets

Abstract

Most research evaluating the potential of mangroves as a sink for atmospheric carbon has focused on carbon burial. However, the few studies that have quantified lateral exchange of carbon and alkalinity indicate that the dissolved carbon and alkalinity export may be several-fold more important than burial. This study aims to investigate rates and drivers of alkalinity, dissolved carbon and greenhouse gas fluxes of the mangrove-dominated Shark River estuary located in the Everglades National Park in Florida, USA. Time series and spatial surveys were conducted to assess total alkalinity (TAlk), organic alkalinity (OAlk), dissolved inorganic carbon (DIC), dissolved organic carbon (DOC), carbon dioxide (CO_2), methane (CH_4) and nitrous oxide (N_2O). Dominant metabolic processes driving dissolved carbon and greenhouse gas dynamics varied along the estuarine salinity gradient. Dissolved carbon and greenhouse gas concentrations were strongly coupled to porewater input, which was examined using radon-222. Shark River was a source of CO_2 (92 mmol/m^2/d), CH_4 (60 µmol/m^2/d) and N_2O (2 µmol/m^2/d) to the atmosphere. Dissolved carbon export (DIC = 142 mmol/m^2/d, DOC = 39 mmol/m^2/d) was several-fold higher than burial (~28 mmol/m^2/d) and represents an additional carbon sink. Furthermore, the estuary was a source of TAlk (97 mmol/m^2/d, normalised to mangrove area) to the coastal ocean, potentially buffering coastal acidification. Organic alkalinity was also exported to the coastal ocean (1.9 mmol/m^2/d, normalised to mangrove area). By integrating our results with previous studies, we argue that alkalinity, dissolved carbon and greenhouse gas fluxes should be considered in future blue carbon budgets.

Plain language summary

Mangroves mitigate climate change by capturing carbon dioxide from the atmosphere. Much research effort has gone into quantifying how much carbon is stored in mangrove soils. However, less is known about the fate and magnitude of dissolved carbon fluxes. This study investigated dissolved carbon and greenhouse gas fluxes at the mangrove-dominated Shark River located in the Everglades National Park in Florida, USA. To examine dissolved carbon and greenhouse gas fluxes, we conducted temporal as well as spatial measurements. Our results showed that dissolved carbon and greenhouse gases varied strongly within the study area. Shark River was a source of greenhouse gas emissions to the atmosphere. However, greenhouse gas fluxes were small compared to dissolved carbon export. Dissolved carbon export was several-fold higher than carbon storage in soils. Therefore, more research is required to evaluate the role of dissolved carbon export as a mangrove carbon sink.

1 Introduction

Mangroves play a disproportionately large role in the coastal carbon cycle. Carbon storage in mangroves is exceptionally high compared to other forest ecosystems (Donato et al., 2011). Globally, mangrove soils store ~2.6 Pg C, which is equal to 9.5 Pg of CO_2 (Atwood et al., 2017) and the global carbon burial rate is estimated to be ~26 Tg C/y (Breithaupt et al., 2012). The blue carbon policy framework, which is increasingly used to protect and restore coastal ecosystems, focuses on carbon burial of mangroves and other vegetated coastal habitats. However, the carbon sink capacity of mangroves extends beyond carbon burial (Maher et al., 2018). Part of the buried carbon is remineralized and exported as dissolved carbon (Friesen et al., 2018; Maher et al., 2013a), which is largely unaccounted for in current blue carbon budgets. Furthermore, carbon remineralization results in greenhouse gas emissions, which partly offset carbon sequestration (Rosentreter et al., 2018b). To date, there are very few studies that examine and integrate all aspects of mangrove carbon cycling and their role in mitigating climate change, including carbon burial, carbon remineralization and subsequent lateral export, as well as greenhouse gas emissions.

Whether mangroves act as source or sink for greenhouse gas emissions appears to vary strongly between sites. A portion of the carbon fixed by mangroves is recycled as CO_2 to the atmosphere. The global average CO_2 emission by mangroves is estimated to be 34 ± 5 Tg C/y (Rosentreter et al., 2018a), which is slightly higher than estimated global carbon burial rates in mangroves (Breithaupt et al., 2012). Compared to CO_2, total methane (CH_4) emissions (water and sediment fluxes) by mangroves are thought to be small (0.273 ± 0.053 Tg C/y) (Rosentreter et al., 2018b). Nonetheless, accounting for CH_4 emissions is important due to CH_4 having a higher global warming potential than CO_2 (IPCC, 2014). Nitrous oxide (N_2O), which is an even stronger greenhouse gas than CH_4, is believed to be emitted at rates of 0.01 – 0.09 Tg N/y by mangroves globally (Murray et al., 2015), but pristine mangroves can also act as N_2O sink (Maher et al., 2016).

In contrast to greenhouse gas emissions, which offset carbon sequestration, the lateral export of remineralized carbon may enhance the carbon sink associated with mangroves. In mangroves, carbon, which is mainly remineralized via sulfate reduction and aerobic respiration, is predominantly exported as dissolved inorganic carbon ($DIC = CO_2 + HCO_3^- + CO_3^{2-}$) and to a lesser extent as dissolved organic carbon (DOC) (Faber et al., 2014; Ho et al., 2017; Maher et al., 2013a; Taillardat et al., 2018). The global DOC exported by mangroves is estimated to be 24 ± 21 Tg C/y (Bouillon et al., 2008). Despite the important role of DIC, current global estimates (43 ± 12 Tg C/y) for mangrove DIC export, which are twice as high as global mangrove carbon burial rates, are derived from only six Australian mangrove creeks (Sippo et al., 2016). This limited spatial coverage of mangrove DIC export estimates represents a major gap in developing a holistic understanding of global mangrove carbon cycling. During export to the coastal ocean, DIC partly outgasses as CO_2 to the atmosphere, whereas carbonate alkalinity ($HCO_3^- + CO_3^{2-}$) effectively remains dissolved in the ocean with an oceanic residence time of ~ 100,000 years (Emerson & Hedges, 2008). In addition to being a long-term carbon sink, total alkalinity (TAlk) exported to coastal waters may help buffer acidification in near-shore coastal waters (Faber et al., 2014; Sippo et al., 2016).

An understudied component of TAlk is organic alkalinity (OAlk), which contributes to TAlk when organic substances are present. Previous studies have found significant contributions of OAlk in rivers (Hunt et al., 2011), estuaries (Cai et al., 1998; Tishchenko et al., 2006), coastal waters (Hernández-Ayon et al., 2007; Hunt et al., 2011; Ko et al., 2016), and the open ocean (Fong & Dickson, 2019). In the coastal and marine environment, OAlk is produced by photosynthesis, for instance by phytoplankton (Kim & Lee, 2009) and algae

(Hernández-Ayon et al., 2007), or by carbon remineralization (Lukawska-Matuszewska et al., 2018). To our knowledge, research investigating OAlk in mangroves is limited to one study, which reported OAlk values up to 47 µmol/kg for seven point measurements (Yang et al., 2015).

This study aims to update the mangrove carbon budget, with a specific focus on aquatic exports, by examining alkalinity, dissolved carbon and greenhouse gas fluxes at the mangrove-dominate Shark River located in the Everglades National Park Florida. We quantified estuarine fluxes and evaluated their underlying drivers, such as carbon mineralization and porewater inputs, by applying contrasting spatial surveys and time series approaches. Furthermore, we present the first study analysing the dynamics and relevance of OAlk in mangrove-dominated estuaries.

2 Methods

2.1 Study site

Shark River is located in Everglades National Park, South Florida (Figure 1) and flows into the Gulf of Mexico. The subtropical climate of South Florida is characterised by a dry season from November to April (average monthly rainfall 54 mm) and a wet season from May to October (average monthly rainfall 189 mm). Average monthly minimum and maximum temperatures range between 12 and 34 °C (Southeast Regional Climate Center, http://www.sercc.com). The area is subject to a semi-diurnal tidal regime, with a mean tidal amplitude of 0.5 – 1 m. Shark River is surrounded by a large mangrove forest (144,447 ha), which has a net ecosystem production (NEP) of 1170 ± 127 gC/m^2/y (Barr et al., 2010). The mangrove forest is dominated by *Rhizophora mangle*, *Avicennia germinans*, *Laguncularia racemose*, and *Conocarpus erectus* (Chen & Twilley, 1999). The freshwater reaches of the low-lying Shark River Slough are comprised of freshwater marshes, which are dominated by *Cladium jamaicense* (Olmsted & Armentano, 1997). The underlying geology of the study area is characterized by a flat carbonate platform formed during the late Mesozoic and the Cenozoic (Petuch & Roberts, 2007).

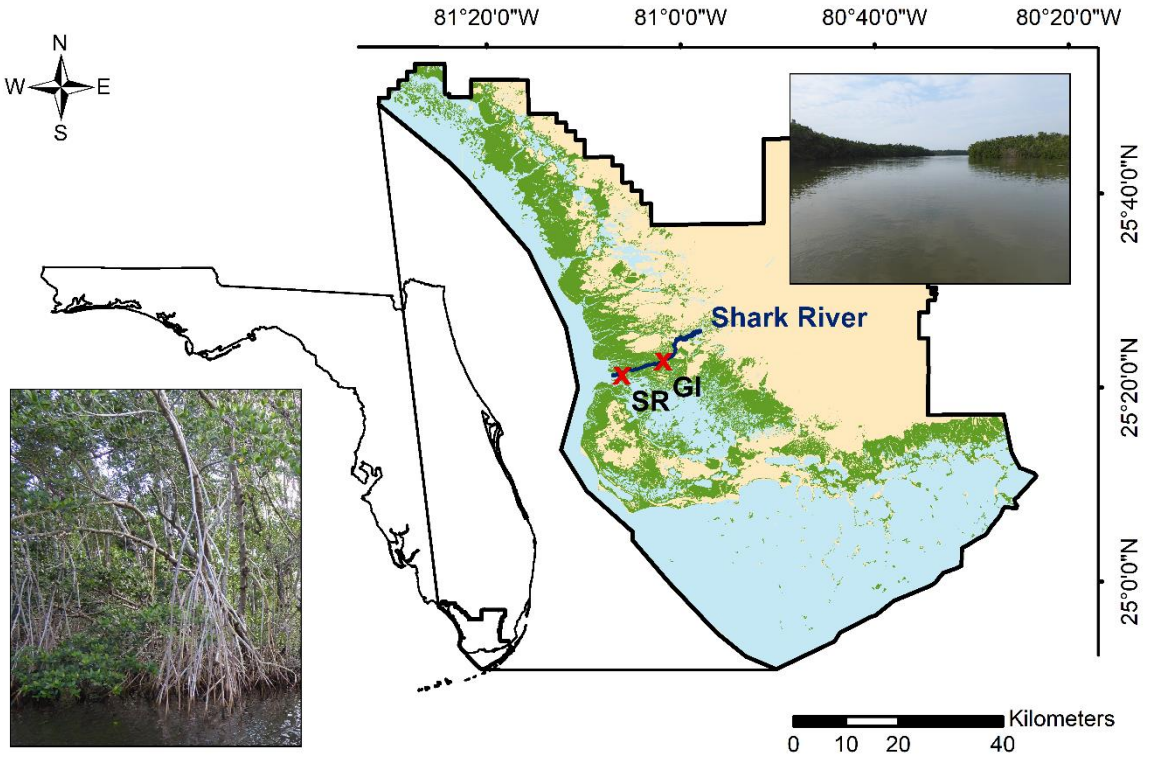

Figure 1. Map presenting mangrove cover (green), time series stations (red crosses) at Shark River within Everglades National Park (black border). Photographs show the dense mangrove forest fringing Shark River.

2.2 Sample collection and analysis

Two longitudinal surveys (SV1, SV2; ~15 km) and two 30 h time series were conducted at Shark River between the 21st and 26th November 2018 (Figure 1). The time series stations are named according to the water quality stations managed by the National Park Service (NPS). The upstream time series station is adjacent to Gunboat Island (GI) (25.3782, -81.0295) and the downstream time series station is towards the mouth of Shark River (SR) (25.3541, -81.1005). Surface water was analysed by automated, continuous

underway measurements as well as by discrete measurements on an hourly basis during the time series measurements and approximately every two salinity units during the spatial surveys.

Surface water from a water depth of approximately 0.5 m was continuously pumped into the on-board measurement setup. Salinity (± 0.01) and water temperature (± 0.002 °C) were measured using a thermosalinograph (SBE 45 MicroTSG). A ion-sensitive field-effect transistor (Honeywell Durafet II) was used to determine pH (± 0.005) as described by Martz et al. (2010). Dissolved oxygen (DO, ±0.06%) was measured with an oxygen optode (Aanderaa 3835) calibrated against Winkler titration. Fluorescent dissolved organic matter (fDOM) was analysed with a fluorometer on a multiparameter Sonde (YSI EXO2), which has a detection limit of 0.07 ppb QSE. Dissolved inorganic carbon samples were acidified in a DIC analyser as described by Friederich et al. (2002), to transfer all carbonate species into CO_2, and subsequently analysed with a non-dispersive infrared absorption (NDIR) detector (LI-COR LI-7000), with a precision better than 0.1%.

Continuous CO_2, N_2O, CH_4 (1 min intervals) and radon-222 (^{222}Rn, min intervals) concentrations were measured via a showerhead equilibrator coupled to gas analysers (Santos et al., 2012). Concentrations of CO_2 and CH_4 were analysed during SV1 and time series at GI with a mobile gas concentration analyser (Picarro GasScouter^{TM} G4301) with a raw precession of 0.4 ppm and 3 ppb, respectively. Nitrous oxide concentrations (±2 ppb), as well as CO_2 (±10 ppm) and CH_4 (±10 ppb) concentrations for SV2 and SR time series, were analysed with by cavity ring-down spectroscopy (Picarro G2308) (Maher et al., 2013b). A radon detector (Durridge RAD7) was used to measure ^{222}Rn (Burnett et al., 2001). Equilibration times of all gases were corrected according to Webb et al. (2016).

For TAlk and OAlk analysis, samples were filtered with 0.7 µm GFF filters and measured within one day, using a titrator (Metrohm 888 Titrando with Tiamo light), which has a precision better than 5 µM. Deviations and drifts in the acid concentration (0.05 M hydrochloric acid) were accounted for, using certified reference materials (CRM batch 175 and CRM batch 178) according to Dickson (2010). The method developed by Cai et al. (1998) was adapted for OAlk determination. Following the first Gran titration, which determines TAlk, samples were purged with high purity nitrogen for five minutes to remove the CO_2 and then back-titrated to the original pH with sodium hydroxide (0.05 M). Subsequently, a second Gran titration was undertaken on the sample, which determines the non-carbonate alkalinity. To calculate OAlk, results were corrected for borate alkalinity, which was calculated from TAlk, pH, temperature and salinity using CO2SYS (Lewis & Wallace, 1998). For DOC analysis, samples were filtered with 0.7 µm GFF filters, preserved with phosphoric acid and analysed with a total organic carbon analyser (Shimadzu TOC-L CSH/CSN), which has a precision better than 2%.

2.3 Calculations

Estuarine input concentrations of dissolved parameters were estimated by a linear mixing model (Kaul & Froelich, 1984). Theoretical linear mixing lines were aligned to observed values at lowest and highest salinities, representing freshwater and seawater endmembers, and the deviation between conservative mixing values and measured values was determined. The deviation values were integrated over the entire survey and divided by the salinity range to get input concentrations. In order to examine lateral export values, the estuarine input concentration was multiplied by the water volume (9400000 m^3) and divided

by the water residence time (4.88 d), which was calculated by applying an equation developed for Shark River by Ho et al. (2016):

$$\tau = 3.678 + 26.718e^{-0.367Q} \quad (1)$$

Where τ is the residence time and Q is the tidally filtered discharge at Gunboat Island (U.S. Geological Survey, 2018). Rates were normalized to the associated tidally inundated area (15.9 km^2) for Shark River (Ho et al., 2017) to scale fluxes to mangrove area for comparison with previous studies. Due to the high uncertainty about this area, ranges for areal fluxes were determined by using half and twice the size of the inundated mangrove area.

In addition to the Lagrangian approach, an Eulerian approach was applied to quantify lateral fluxes. Lateral TAlk, DIC and DOC fluxes were calculated by multiplying concentrations, which were sampled during time series measurements, with discharge at 15-minute intervals. To attain higher temporal resolution for TAlk, OAlk and DOC flux rates, TAlk was calculated using CO2SYS from high-resolution measurements of DIC and pH (Pierrot et al., 2009), and DOC as well as OAlk were calculated from fDOM using linear relationships (see discussion). Concentrations were averaged for each time step. Discharge values were retrieved from the U.S. Geological Survey station at Gunboat Island (U.S. Geological Survey, 2018). Start and end time were adjusted to balance the water volumes and included two complete tidal cycles. Positive values indicate fluxes directed towards the ocean. To get areal rates (i.e., $mmol/m^2/d$), total fluxes have been scaled to the estimated inundated area between the time series stations (8.7 km^2), whose boundaries were, due to the lack of a high-resolution DEM, estimated to be halfway to the next watercourse. Similar to the Eulerian approach, uncertainties on the areal fluxes were accounted for by halving and doubling inundation area.

Concentrations of CO_2, CH_4 and N_2O were corrected for water vapour removal and converted to partial pressure according to the methods detailed in Pierrot et al. (2009). Air-water gas fluxes of O_2, CO_2, CH_4 and N_2O were determined, as product of the gas transfer velocity, the solubility coefficient and the difference in the air-water partial pressure:

$$F_{CO2} = k_{CO2}\, K_0\, (pCO_{2(water)} - pCO_{2(air)}) \quad (2)$$

where F_{CO2} is the CO_2 flux ($mmol/m^2/d$), k_{CO2} is the gas transfer velocity, K_0 is the solubility coefficient, $pCO_{2(water)}$ is the partial pressure of CO_2 in water and $pCO_{2(air)}$ is the partial pressure of CO_2 in air. The same calculation was applied to determine oxygen (O_2), CH_4 and N_2O air-water fluxes. The solubility coefficients were calculated as a function of salinity and temperature for O_2 (Benson & Krause, 1984), CO_2 (Weiss, 1974), CH_4 (Wiesenburg & Guinasso Jr, 1979) and N_2O (Weiss & Price, 1980). Atmospheric partial pressures of 412 µatm for CO_2, 1.8 µatm for CH_4 and 0.33 µatm for N_2O were used. According to the convention, positive values presenting a flux towards the atmosphere. The gas transfer velocity was calculated:

$$k_{CO2} = k(600)\, (Sc_{CO2}/600)^{-0.5} \quad (3)$$

where k(600) is the gas transfer velocity normalized to a Schmidt number of 600 and Sc_{CO2} is the Schmidt number, which was calculated as function of temperature and salinity assuming a linear dependence of the Schmidt number on salinity (Wanninkhof, 2014). Integrating wind speed, current velocity and water depth, k(600) was calculated according to Ho et al. (2016), who conducted deliberate gas tracer experiments in the Shark River to derive an empirical equation for k(600) determination:

$$k(600) = 0.77v^{0.5}h^{-0.5} + 0.266u_{10}^{2} \quad (4)$$

where v is the current velocity, h is the mean depth of Shark River (2.8 m) (Ho et al., 2014) and u_{10} is the wind speed at 10 m height, which was recorded on site with a weather station (ATMOS 41). Gas fluxes were interpolated to the water area of the entire Shark River (2.2 km^2) and the area between the time series stations (0.9 km^2), using the spatial analyst tool of ArcGIS 10.6.1 (Maher & Eyre, 2012).

Statistical analysis was conducted in SigmaPlot 14.0. The Pearson correlation coefficients (r) were determined for alkalinity, dissolved carbon, greenhouse gases and the explanatory variables (salinity, ^{222}Rn and DO) to evaluate underlying drivers. The probability levels are presented as * if $p < 0.05$, ** if $p < 0.01$ and *** if $p < 0$ .001. For the linear regressions between OAlk, DOC and fDOM, coefficients of determination (R^2) have been reported.

3 Results

The spatial variations in alkalinity, dissolved carbon and greenhouse gases along the Shark River show clear estuarine trends (Figure 2). Within the mangrove zone, TAlk, DIC and CO_2 peak at brackish waters, whereas DOC is highest at upstream freshwater sites. In comparison, CH_4 and N_2O show less distinct patterns, but decrease, like all parameters, towards the Gulf of Mexico. It has to be noted that Shark River flows through a very flat terrain and is highly connected with other streams and creeks.

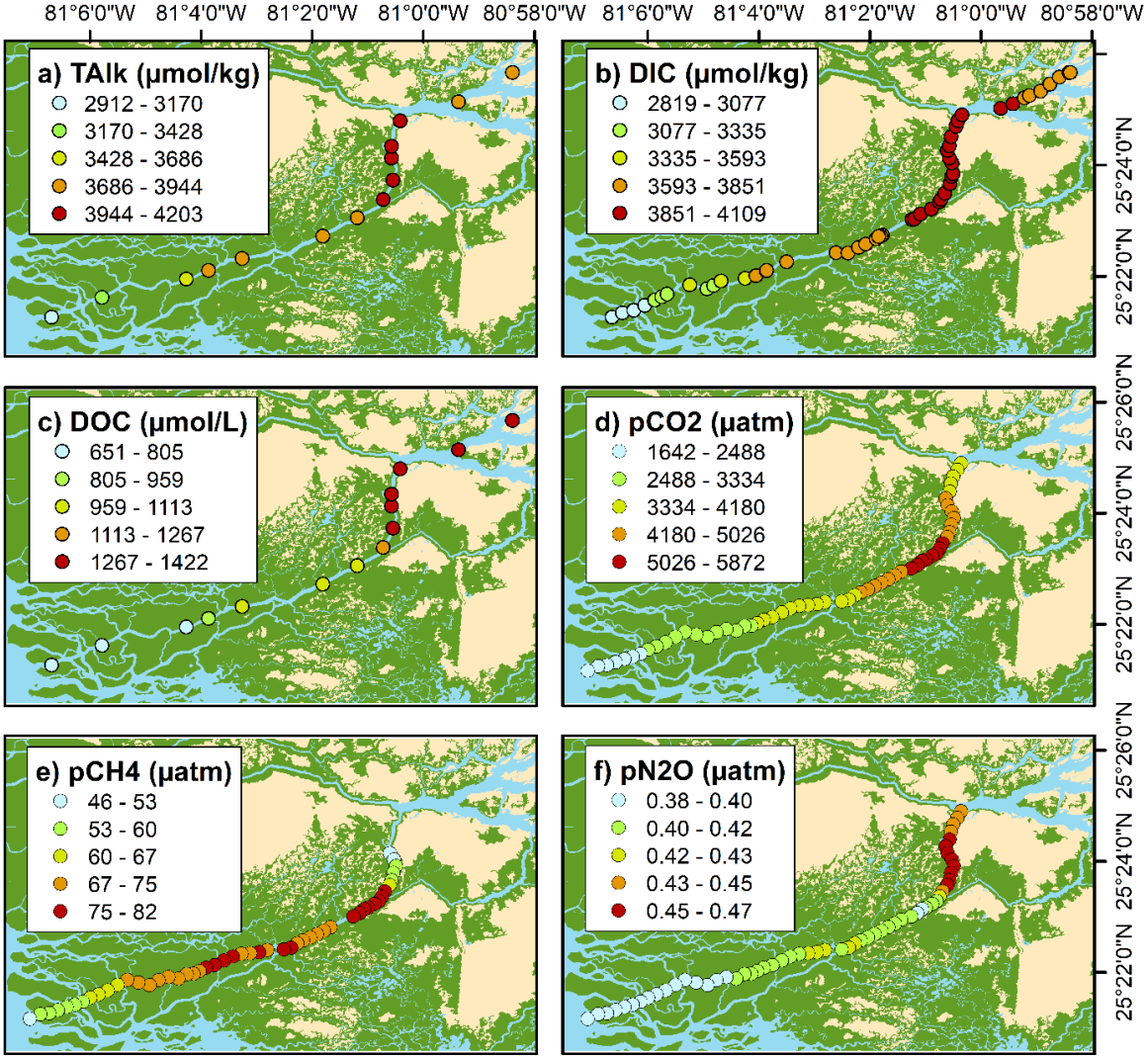

Figure 2. Maps of Shark River showing total alkalinity (TAlk, a), dissolved inorganic carbon (DIC, b), dissolved organic carbon (DOC, c) recorded during the first survey (SV1) and the partial pressure of carbon dioxide (pCO_2, d), methane (pCH_4, e) and nitrous oxide (pN_2O, f) recorded during the second survey (SV2).

Ranges and trends of all measured parameters varied little between the two spatial surveys (Figure 3). Dissolved oxygen saturation (36 – 82%) and pH (7.4 – 7.8) showed a concave down pattern along the salinity gradient, which ranged from 0.7 to 29. The average water temperature during SV1 (25.9 °C) was slightly higher than during SV2 (25.2 °C). Radon declined from 5014 dpm/m^3 in brackish waters to 329 dpm/m^3 towards the river mouth. Similar to ^{222}Rn, pCO_2 (1643 – 5873 µatm) and pCH_4 (46 – 82 µatm, 53 – 105 nM) increased at intermediate salinities. In contrast, N_2O (0.36 – 0.49 µatm, 7 – 12 nM) decreased slightly towards higher salinity. Both, TAlk and DIC showed similar concentrations and trends ranging from 2913 to 4255 µmol/kg and from 2753 to 4277 µmol/kg, respectively.

Concentrations of OAlk (0 – 81 µmol/kg) decreased almost linearly with increasing salinity, while DOC (604 – 1422 µmol/L) and fDOM (39 – 161 ppb) were non-conservative. During SV2 wind speed varied between 0.81 and 1.88 m/s.

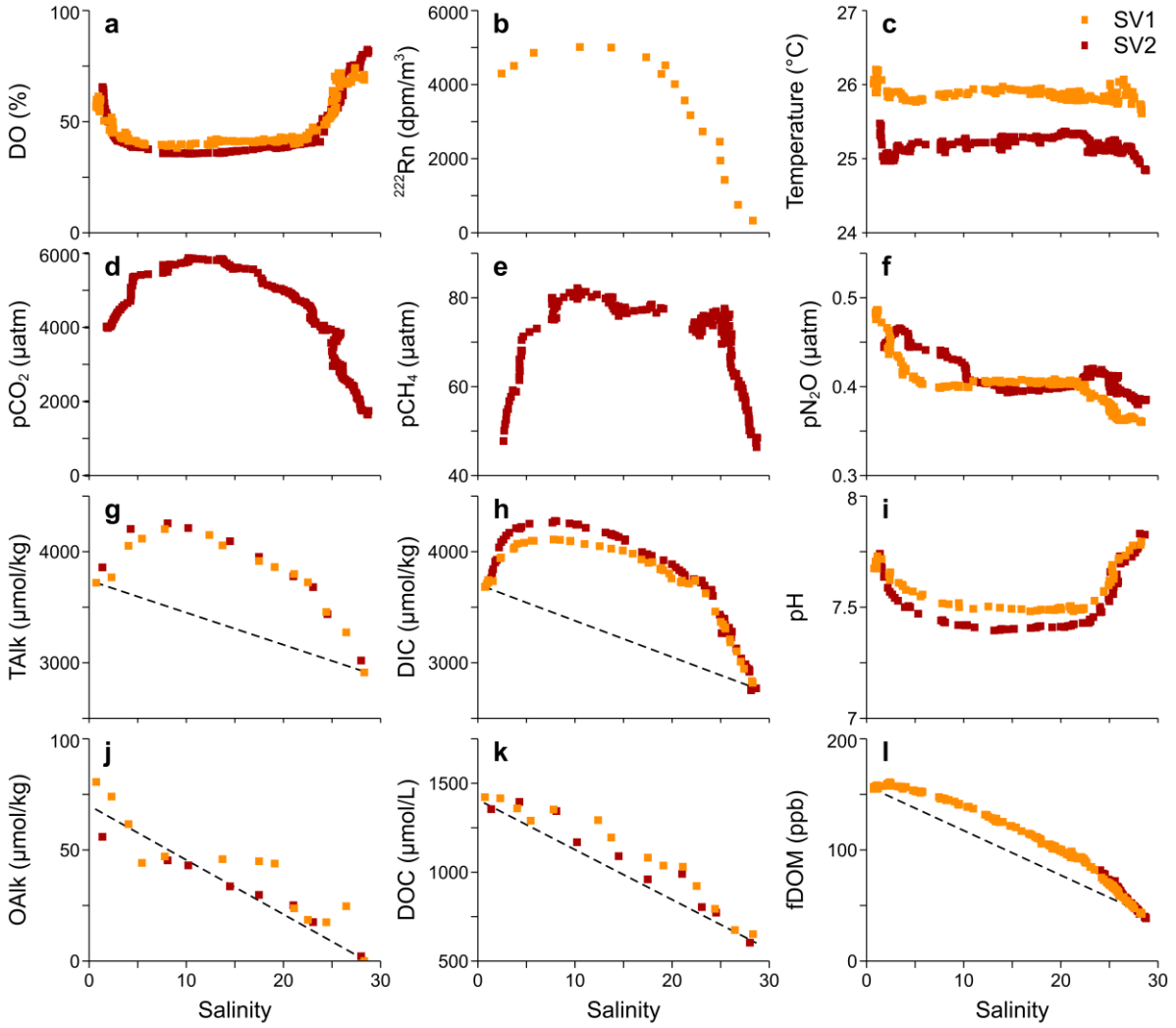

Figure 3. Biochemical parameters were measured during two spatial surveys along the Shark River. Oxygen (DO, a), radon-222 (^{222}Rn, b), temperature (c), carbon dioxide (pCO_2, d), methane (pCH_4, e), nitrous oxide (pN_2O, f), total alkalinity (TAlk, g), dissolved inorganic carbon (DIC, h), pH (i), organic alkalinity (OAlk, j), dissolved organic carbon (DOC, k) and fluorescent dissolved organic matter (fDOM, l) are plotted against salinity. Dashed lines represent linear mixing curves.

Positive deviations from linear mixing curves indicate inputs of alkalinity and dissolved carbon (Figure 3). Input concentrations of TAlk (527 µmol/kg) and DIC (664 µmol/kg) were high compared to DOC (100 µmol/L) and fDOM (19 ppb). At the brackish section, the estuary was a sink for OAlk, but turned into an OAlk source at salinities above 10 (5 µmol/kg). The greenhouse gases CO_2 and CH_4 showed a distinct non-conservative behaviour, suggesting a source within the estuary, whereas N_2O exhibited an alternating source-sink behaviour.

The two time series stations were exposed to contrasting salinity ranges, with values ranging from 3 to 22 at GI and from 26 to 29 at SR (Figure 4). The upstream site GI experienced freshwater DO input during low tide and seawater DO input during high tide (31 - 41% saturation), and pH (7.4 – 7.6) was negatively correlated with salinity with small peaks at high tide. Being mainly controlled by oceanic influences, DO (53% - 85% saturation) and

pH (7.6 – 7.9) changed simultaneously with salinity at SR. Water temperatures were similar for both time series stations, averaging 24.8 °C. At the GI site, ^{222}Rn reached twofold higher values (5648 – 9969 dpm/m_3) compared to the SR site (1437 – 6515 dpm/m^3). During the times series at GI, discharge ranged from -186 to 189 m^3/s and during time series at SR from -239 to 218 m^3/s.

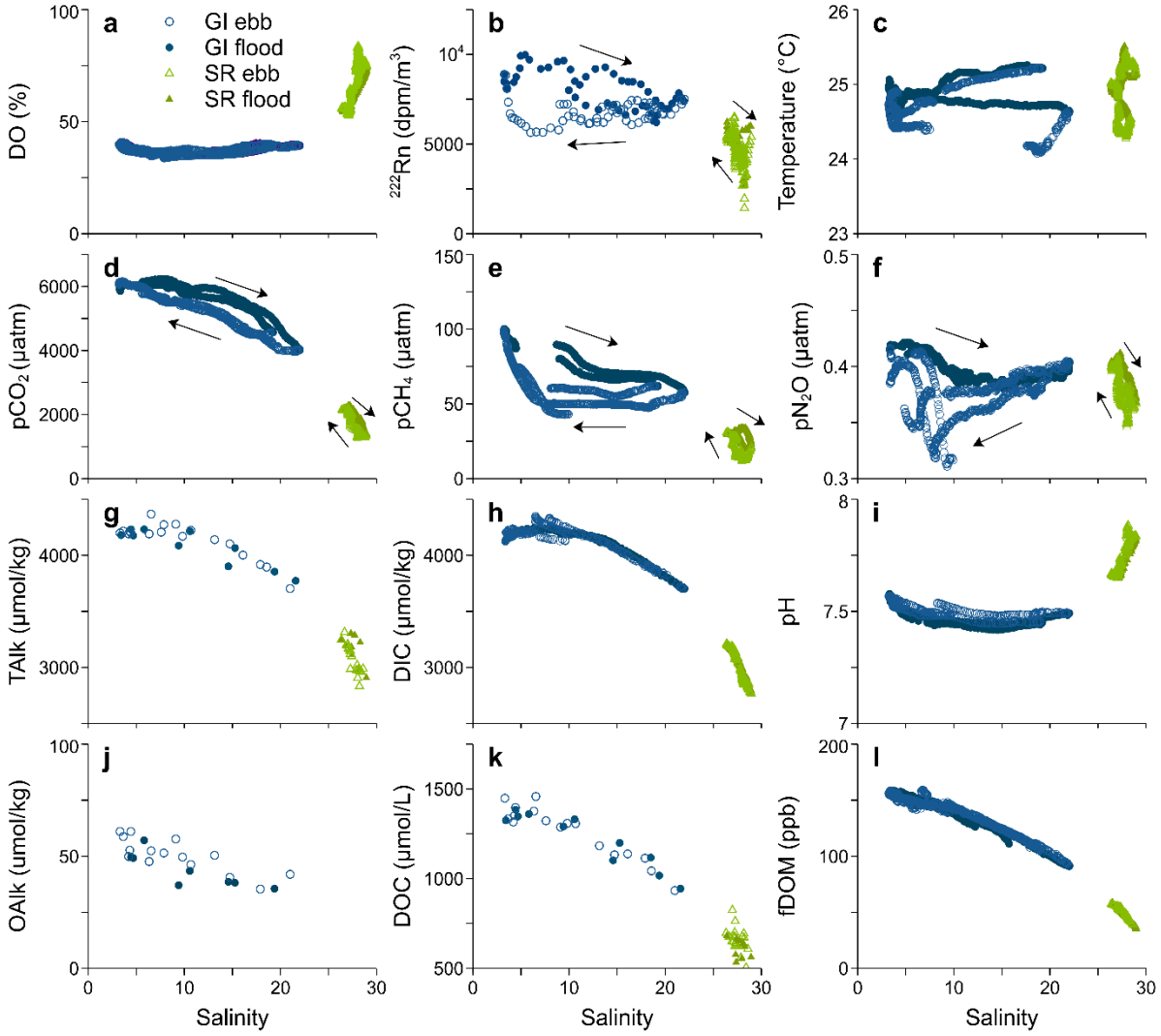

Figure 4. Biochemical parameters were measured at upstream (GI) and downstream (SR) time series stations at Shark River. Oxygen (DO, a), radon-222 (^{222}Rn, b), temperature (c), carbon dioxide (pCO_2, d), methane (pCH_4, e), nitrous oxide (pN_2O, f), total alkalinity (TAlk, g), dissolved inorganic carbon (DIC, h), pH (i), organic alkalinity (OAlk, j), dissolved organic carbon (DOC, k) and fluorescent dissolved organic matter (fDOM, l) are plotted against salinity.

At both stations, CO_2, CH_4, N_2O, TAlk, DIC, DOC and fDOM were inversely related to salinity (Figure 4). During time series at GI, pCO_2 (3976 – 6240 µatm) and pCH_4 (43 – 100 µatm, 56 – 134 nM) were much higher compared to pCO_2 (1257 – 2272 µatm) and pCH_4 (12 -34 µatm, 14 – 39 nM) at SR. In contrast, N_2O reached almost similar values at both stations (0.31 – 0.42 µatm, 7 – 10 nM). At GI, TAlk ranged from 3704 – 4368 µmol/kg and at SR from 2832 – 3315 µmol/kg. Concentrations of DIC ranged from 3702 – 4348 µmol/kg at GI and from 2765 – 3214 µmol/kg at SR. Due to equipment failure, OAlk data are only available for the GI site (35 - 61 µmol/kg). Concentrations of DOC were two times and fDOM was three times higher at GI (934 – 1458 µmol/L, 91 – 159 ppb) compared to SR (504 – 825 µmol/L, 35 – 59 ppb).

Comparing time series with the spatial surveys, DO, TAlk, DIC and DOC concentrations and trends were similar, whereas ^{222}Rn and the greenhouse gases showed different trends. Unlike the spatial surveys, ^{222}Rn, CO_2, CH_4 and N_2O followed a hysteresis pattern during the time series measurements, reaching higher values at a given salinity during flood tide at both stations. The hysteresis was less developed for CO_2 than for CH_4, N_2O and ^{222}Rn. During time series, ^{222}Rn values were at least twice higher than during the spatial surveys.

Shark River was a source for all studied greenhouse gases and a sink for DO (Table 1). Referring to the water area (0.94 km^2) between the time series stations, DO uptake by the river (-2.1 x 10^5 mol/d) was threefold higher than CO_2 emissions (6.4 x 10^4 mol/d). In comparison, CH_4 emissions (53 mol/d) played only a minor role and N_2O emissions (1 mol/d) were negligible.

During the time series measurements, dissolved carbon and alkalinity were exported to the ocean (Table 1). The fluxes at upstream GI were considerably smaller, constituting only 4 – 15% of the fluxes at downstream SR. At GI, DIC and DOC fluxes were comparable, whereas at SR the DIC (76%) was the major dissolved carbon export. Fluxes of DIC and TAlk were similar (1 x 10^6 mol/d) at SR, but at GI DIC (5 x 10^4 mol/d) was lower than TAlk (1 x 10^5 mol/d). At both sites, the OAlk flux accounted for 2% of the TAlk flux and 5% of the DOC flux. The difference between the fluxes at both time series stations is equal to the input by the mangrove-dominated area in between. The estuarine input was 1 x 10^6 mol/d of DIC, 8 x 10^5 mol/d of TAlk, 3 x 10^5 mol/d of DOC and 2 x 10^4 mol/d of OAlk. The DIC input was 13 times higher than the CO_2 emission and 78% of the dissolved carbon input.

Fluxes estimated with the Lagrangian approach for the entire Shark River, were similar to the fluxes acquired during the time series (Table 1). Areal rates were slightly smaller for the Lagrangian approach, which included the entire estuary, than for the Eulerian approach, which covered the mangrove-dominated sections of the estuary.

Table 1. Air-water fluxes are shown for entire Shark River and the mangrove-dominated area between time series stations. Lateral fluxes are presented for at the upstream station (GI), the downstream station (SR) and the input by the mangrove-dominated area between the time series stations using the Eulerian and Lagrangian approach. Uncertainty bands for areal rates are shown in brackets.

Air-water	DO flux	CO_2 flux	CH_4 flux	N_2O flux
Shark River (mol/d)	-6.3×10^5	2.0×10^5	136	3.6
Shark River (mmol/m^2/d)	-285	92	0.06	0.002
Mangrove area (mol/d)	-2.1×10^5	6.4×10^4	53	1.0
Mangrove area (mmol/m^2/d)	-222	68	0.06	0.001

Lateral	DIC flux	TAlk flux	DOC flux	OAlk flux
GI station (mol/d)	5.5×10^4	1.3×10^5	5.5×10^4	2.9×10^3
SR station (mol/d)	1.3×10^6	9.7×10^5	4.0×10^5	2.0×10^4
Eulerian (mol/d)	1.2×10^6	8.4×10^5	3.4×10^5	1.7×10^4
Eulerian (mmol/m^2/d)	142 (71 – 284)	97 (48 – 193)	39 (20 – 79)	1.9 (1.0 – 3.9)
Lagrangian (mol/d)	1.3×10^6	1.0×10^6	1.9×10^5	9.6×10^3
Lagrangian (mmol/m^2/d)	80 (40 – 161)	64 (32 – 128)	12 (4 – 24)	0.6 (0.3 – 1.2)

Pearson's correlation coefficients between alkalinity, dissolved carbon, greenhouse gases and the explanatory variables salinity, ^{222}Rn and DO provide insights into underlying drivers of estuarine processes (Table 2). Salinity was a good predictor (negatively correlated) for most parameters. Correlations between CH_4, N_2O and salinity were less evident during the spatial surveys and GI, respectively. During the spatial surveys, the natural groundwater tracer ^{222}Rn was highly correlated ($r \geq 0.78$) with all parameters. However, the relationship between ^{222}Rn and measured parameters was not as strong during the time series measurements, except for CH_4 ($r > 0.70$). Oxygen (a proxy for aerobic metabolism) was negatively correlated to parameters measured during the spatial surveys and the SR time series. In contrast, DOC and OAlk had weaker correlations with DO.

Table 2. Pearson correlations between dissolved carbon, alkalinity, greenhouse gases and the explanatory variables for upstream (GI) and downstream (SR) time series and both spatial surveys (SV).

	Variables	DIC	DOC	TAlk	OAlk	CO_2	CH_4	N_2O
SV	Salinity	-0.73***	-0.96***	-0.71***	-0.92***	-0.66***	-0.23***	-0.81***
	^{222}Rn	0.97***	0.92***	0.97***	0.81**	NA	NA	0.78***
	DO	-0.90***	-0.50*	-0.84***	-0.30	-0.96***	-0.70***	-0.38***
GI	Salinity	-0.89***	-0.94***	-0.86***	-0.79***	-0.90***	-0.41***	0.05
	^{222}Rn	0.05	0.23	0.07	0.04	0.34***	0.70***	0.56***
	DO	-0.64***	-0.37	-0.49*	-0.14	-0.63***	0.17***	0.46***
SR	Salinity	-0.96***	-0.48**	-0.74***	NA	-0.87***	-0.65***	-0.68***
	^{222}Rn	0.52***	0.12	0.55**	NA	0.63***	0.80***	0.53***
	DO	-0.94***	-0.44*	-0.89***	NA	-0.97***	-0.84***	-0.82***

4 Discussion

4.1 Relevance and proxies of organic alkalinity

Despite the potential relevance of OAlk, many studies do not directly measure but calculate OAlk (Hammer et al., 2017; Hernández-Ayon et al., 2007; Kim & Lee, 2009; Kuliński et al., 2014; Lukawska-Matuszewska et al., 2018). Organic alkalinity is often estimated as the difference between observed and calculated TAlk, which is determined by the carbonate system and can therefore be calculated from pH, DIC or pCO_2. Testing all available dissociation constants in CO2SYS, constants derived from Millero (2010), which were determined for estuarine waters, were found to be the best fit for OAlk calculations at Shark River. However, there were substantial discrepancies between calculated and measured OAlk (Figure 5a). Along the salinity gradient, the slopes of salinity versus calculated OAlk were higher than for salinity versus measured OAlk, resulting in overestimation at low and underestimation at high salinities (Figure 5b). This salinity dependant discrepancy between measured and calculated OAlk suggests that the published dissociation constants may not be applicable for Shark River, where measured TAlk and DIC concentrations were twice as high than concentrations of seawater, which was used for determining dissociation constants (Millero, 2010). It can be concluded that in estuarine systems, either site specific dissociation constants should be developed and verified or OAlk should be measured rather than calculated.

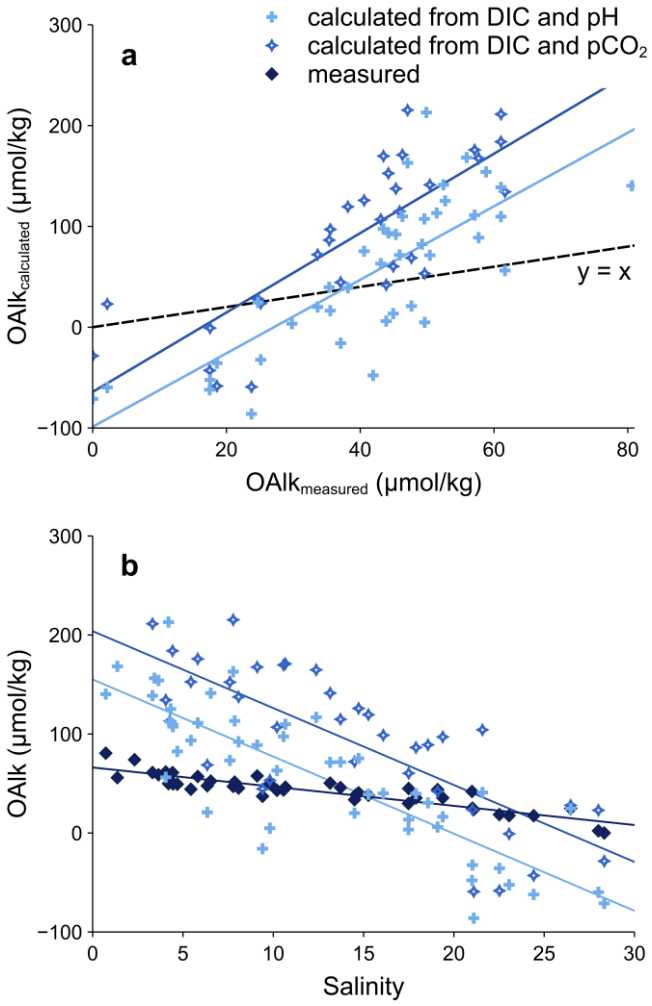

Figure 5. Organic alkalinity was calculated ($OAlk_{calculated}$) as the difference between measured total alkalinity and total alkalinity calculated from dissolved inorganic carbon and pH or dissolved inorganic carbon and the

partial pressure of carbon dioxide. Calculated values differed considerably from measured organic alkalinity ($OAlk_{measured}$) (a). Calculations lead to overestimations at low and underestimations at high salinity (b).

An alternative approach to either laborious OAlk measurements or OAlk calculations is the use of proxies. Exploring the suitability of potential proxies, we found DOC (R^2 = 0.78) to be a good predictor for OAlk (Figure 6). Previous studies similarly suggested a close relationship between OAlk and DOC (Kim & Lee, 2009; Koeve & Oschlies, 2012; Kuliński et al., 2014; Ulfsbo et al., 2015). Conducting spike experiments with artificial seawater, Hammer et al. (2017) found linear relationships between DOC and OAlk, with different slopes for humic (0.1) and fulvic (0.08) substances. The slope at Shark River (0.06) suggests that fulvic substances might contribute more to OAlk than humic substances at this site. Using water of two rivers, an organic matter enrichment experiment showed very similar OAlk-DOC slopes (0.06 and 0.07), but unlike our study, a positive intercept was found (>148) (Kuliński et al., 2014). Compared to other studies, which reported contributions of up to 100% (Cai et al., 1998; Hunt et al., 2011; Kuliński et al., 2014), OAlk at Shark River accounted only for a small share of DOC (4%). The negative intercept for OAlk and DOC regressions demonstrate that for DOC concentrations < 600 µmol/L no OAlk was present, suggesting that all acid functional groups were protonated. The low OAlk contribution to DOC compared to other studies might be due to differences in temperature, salinity, pH and organic compound composition (thus different pk_a values), which affect the acid-base behaviour of organic matter (Cai et al., 1998).

A cost and time efficient alternative to DOC measurements is the use of fDOM sensors, which are increasingly used to monitor DOC at a high temporal resolution (Baker & Spencer, 2004; Suryaputra et al., 2015). In line with previous findings, the present study showed that fDOM was a very good proxy for DOC (R^2 = 0.98) over a broad salinity range (Figure 6). Hence, similar to DOC, fDOM was also a good predictor for OAlk (R^2 = 0.74), thus suggesting that fDOM sensors may be a useful alternative technique for high-resolution OAlk monitoring, but more research needs to be undertaken to confirm the use of fDOM as an OAlk proxy.

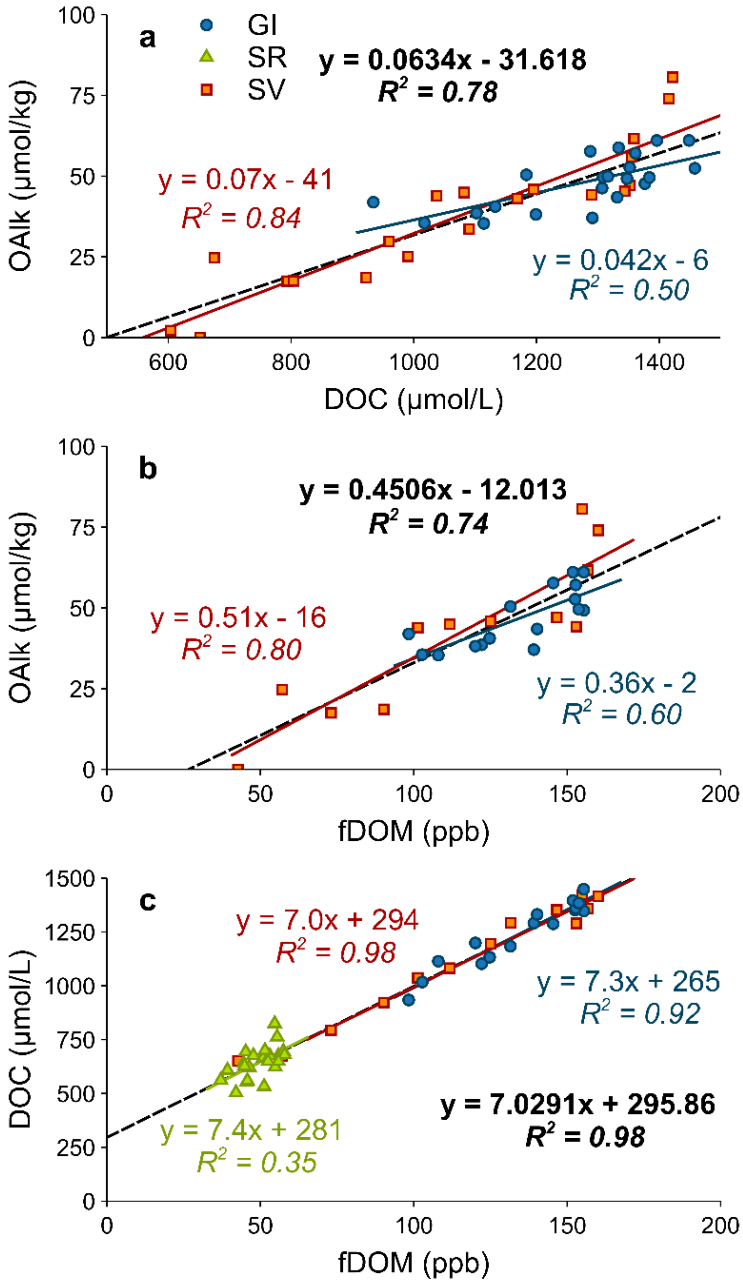

Figure 6. Organic alkalinity (OAlk) was correlated with dissolved organic carbon (DOC, a) and fluorescent dissolved organic matter (fDOM, b). Fluorescent dissolved organic matter was a very good proxy for dissolved organic carbon (c). All linear regressions had probability levels of $p < 0.001$, except for fDOM versus DOC at SR ($p = 0.004$).

Concentrations of OAlk at Shark River (0 – 81 µmol/kg) accounted for ~1% of TAlk and were comparable to literature values for mangroves and other vegetated coastal habitats. Yang et al. (2015) calculated OAlk for seven mangrove sites in the Gulf of Mexico, Florida, reporting values between -16 and 47 µmol/kg for salinities higher than 23. Measuring OAlk along salinity gradients of saltmarsh dominated rivers in Georgia, Cai et al. (1998) found OAlk concentrations reaching from 8 to 112 µmol/L. At a Ramsar site in San Quintín Bay, Mexico, which is vegetated by seagrasses and saltmarshes, OAlk concentrations ranged between 20 – 75 µmol/kg (Hernández-Ayon et al., 2007). The small share of OAlk to TAlk (1%) compared to previous studies (up to 23%) (Cai et al., 1998), is attributed to the higher overall TAlk concentrations (up to 4368 µmol/kg) in Shark River.

Along the salinity gradient, OAlk was removed during early stages of mixing at upstream sites, whereas the mangrove-dominated area represented a net source for OAlk (5 µmol/L). During estuarine mixing, OAlk can be removed by protonation of humic acids (Cai et al., 1998) and organic matter removal driven by photodegradation (Moran et al., 2000), remineralisation (Maher & Eyre, 2010), or flocculation (Sholkovitz et al., 1978). At the mangrove-dominated area between the time series stations, OAlk input exceeded the removal, resulting in a lateral export of OAlk towards the ocean, which accounted for 2% of the TAlk export. However, even small OAlk concentrations can have a large effect on the pH. Calculations showed that the pH of Shark River would be up to 0.3 units lower without the presence of OAlk. Even though it represents only a small proportion of the TAlk pool and fluxes, OAlk may substantially buffer the pH of estuarine and coastal waters. However, how this OAlk affects buffering capacity and pH of estuarine and coastal waters remains challenging to constrain, due to the complex mixture of organic compounds contributing to the OAlk pool with varying pK_a and biogeochemical reactivity (Hu, 2020). Nonetheless, our results suggest that further investigations on OAlk inputs from mangroves is warranted.

4.2 Drivers of alkalinity, dissolved carbon and greenhouse gas dynamics

Despite the comprehensive data acquisition during the measurements presented here, our measurements were undertaken over a short period. Alkalinity, dissolved carbon, and greenhouse gases are known to vary between seasons (Koné & Borges, 2008; Volta et al., 2018) and over spring neap cycles (Call et al., 2015) within mangrove systems. Therefore, while our data provides insights into the flux rates and mechanisms driving carbon and greenhouse gas dynamics in Shark River during the study period, long-term seasonal and interannual variability cannot be assessed.

In estuarine sediments, TAlk, dissolved carbon and greenhouse gases are known to be driven by redox reactions coupled to remineralisation of organic matter (Burdige, 2011). Compared to freshwater and seawater endmembers, estuarine waters of Shark River were strongly depleted in DO, suggesting high aerobic carbon mineralization rates in the mangrove-dominated area. The relative importance of different metabolic processes of carbon remineralisation can be examined through linear regression of salinity normalized TAlk ($TAlk_n$) and salinity normalized DIC (DIC_n) (Bouillon et al., 2007; Friis et al., 2003). The slopes resulting from TA_n and DIC_n regressions are characteristic for the prevailing metabolic process: -0.2 for aerobic respiration, 0.8 for denitrification, 1.0 for sulfate reduction, 2.0 for $CaCO_3$ dissolution, 4.0 for manganese reduction and 8.0 for iron reduction. The slopes found during the spatial surveys (0.87), the GI (0.64) and SR (0.45) time series suggest a combination of aerobic respiration, denitrification, sulfate reduction and carbonate dissolution were likely most dominant (Figure 7). However, denitrification can be neglected, since due to limited nitrate availability, denitrification rates at Shark River are very low (Inglett et al., 2011), explaining also the low N_2O emissions observed during this study. Consequently, aerobic respiration, sulfate reduction and carbonate dissolution were the major metabolic pathways driving TAlk, dissolved carbon and greenhouse gas dynamics at Shark River.

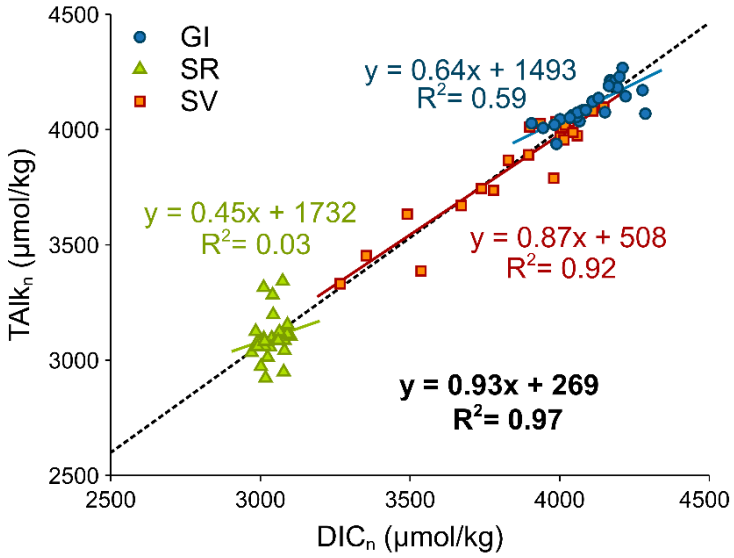

Figure 7. Salinity normalized alkalinity ($TAlk_n$) plotted against salinity normalized dissolved inorganic carbon (DIC_n) for upstream (GI) and downstream (SR) time series measurements and both spatial surveys (SV).

Contributions of metabolic processes strongly differed between the individual measurements. At downstream SR, which had higher DO concentrations, aerobic respiration seemed to play a more dominant role. In contrast, at the upstream site GI and the spatial surveys, sulfate reduction and carbonate dissolution were more important. Since aerobic respiration decouples DIC and TAlk production, $TAlk_n$ and DIC_n were not correlated at SR. In contrast, high correlations at GI and during the surveys suggested similar production processes for TAlk and DIC. Combining both time series measurements and the spatial surveys yields an even higher slope (0.93, Figure 8) than the spatial surveys alone, thus highlighting the overall importance of sulfate reduction and carbonate dissolution within the estuary.

Slopes from $TAlk_n$ and DIC_n regressions reported in previous mangrove studies ranged between 0.44 and 0.92 (Bouillon et al., 2007; Ho et al., 2017; Koné & Borges, 2008; Sippo et al., 2016; Zablocki et al., 2011). The slope during SR time series was at the lower, and during the spatial surveys at the upper end of the previously described values. The fact that the overall slope, combing all measurements, was slightly higher than reported values is possibly due to the additional TAlk production from carbonate dissolution, since Shark River drains at a large carbonate basin. Based on a $\delta^{13}C$ mass balance for Shark River, Ho et al. (2017) estimated that carbonate dissolution accounted for 34% of the estuarine DIC production. If a similar proportion of carbonate dissolution to DIC production occurred during our study, then the proportion of aerobic respiration and sulphate reduction to DIC production would be 34% and 32% respectively (assuming no other major respiration pathways).

Being primarily produced within estuarine sediments, TAlk, dissolved carbon and greenhouse gases are largely derived from porewater, which is constantly being exchanged with surface water via tidal pumping (Call et al., 2015; Chen et al., 2018; Maher et al., 2013a). During the spatial survey, the natural porewater tracer ^{222}Rn peaked at the mid estuary (Figure 3), indicating increased porewater inputs within the mangrove area. Observed ^{222}Rn values, which reached up to ~ 10000 dpm/m^3 during the GI time series, were in the midrange compared to values reported previously (Call et al., 2015; Gleeson et al., 2013; Taillardat et al., 2018; Tait et al., 2016), suggesting exchange rates similar to other mangrove systems. Spanning a latitudinal gradient, Tait et al. (2016) reported mangrove porewater

exchange rates between 2 and 36 cm/d. High porewater exchange rates in mangroves can be a result of macropores, such as those from crab burrows, which expose carbon mineralization products to tidally driven circulation (Stieglitz et al., 2013).

Positive correlations between TAlk, dissolved carbon and greenhouse gases with ^{222}Rn suggest that porewater input was an important driver of carbon cycling at Shark River. Similarly, previous studies reported positive correlations for ^{222}Rn with TAlk, DIC, DOC, CO_2, CH_4 and N_2O in mangroves (Call et al., 2015; Call et al., 2019; Faber et al., 2014; Maher et al., 2013a; Reading et al., 2017; Sadat-Noori et al., 2016; Taillardat et al., 2018). Maher et al. (2013a) found that 89-92% of DOC and 93 – 99% of DIC export from a subtropical mangrove creek was driven by porewater input. Results of Call et al. (2015) showed that porewater exchange controlled CO_2 and CH_4 concentrations with exchange rates driven by tidal amplitude changes over spring-neap cycles. Santos et al. (2019) reported significant porewater fluxes of TAlk (124 ± 131 mmol/m^2/d), DIC (256 ± 203 mmol/m^2/d), DOC (283 ± 190 mmol/m^2/d), CO_2 (120 ± 78 mmol/m^2/d) and CH_4 (1.2 ± 0.8 mmol/m^2/d) at a subtropical mangrove and saltmarsh dominated creek.

During the present study, correlations between ^{222}Rn and all studied parameters were much higher ($r \geq 0.78$) for spatial surveys than for individual time series ($r \leq 0.80$), in part because measured gases, including ^{222}Rn, followed a hysteresis during the time series (Figure 4). Hysteresis for ^{222}Rn, CO_2, CH_4 and N_2O were most probably a result of long equilibration times (30 min for ^{222}Rn and CH_4, 10 min for CO_2 and N_2O) causing overlying signals during turning tides. Since changes from high to low concentrations require longer equilibration times than low to high transitions (Webb et al., 2016), ^{222}Rn and greenhouse gas peaks during low tide were delayed. As a consequence, ^{222}Rn correlated more with CO_2, CH_4 and N_2O during the time series than with dissolved carbon and TAlk, whose analysis do not require equilibration and had thus similar concentrations during spatial surveys and time series (Figure 3 and 4). Moreover, having identical equilibration times (30 minutes), ^{222}Rn and CH_4 correlations were particularly high ($r \geq 0.7$) during the time series compared to all other parameters. An alternative explanation for delayed radon and greenhouse gas peaks during time series include natural processes, such as delayed porewater input (Santos et al., 2019) or different sink processes for dissolved carbon parameters and gases (Sadat-Noori et al., 2016). However, similar trends for dissolved carbon parameters and measured gases during the spatial surveys indicate that methodological reasons are likely responsible for delayed radon and greenhouse gas peaks.

4.3 Lateral carbon fluxes and greenhouse gas emissions

At Shark River, TAlk, DIC and DOC were produced within the estuary and exported to the Gulf of Mexico (Table 1). The two independent methods applied (Lagrangian and Eulerian) were in close agreement, validating the lateral export values and their relative portions. The estuarine carbon export was dominated by DIC (78 – 87%), whereas DOC played only a minor role (13 – 22%). Similarly, previous studies showed that in mangroves most of the dissolved carbon is exported in the form of DIC (Faber et al., 2014; Maher et al., 2018; Maher et al., 2013a; Taillardat et al., 2018). Previous work by Ho et al. (2017), found a similar DIC contribution of 82 – 83% of the dissolved carbon fluxes at Shark River.

Quantification of mangrove contributions is beyond the scope of this study, but using ^{13}C budgets previous studies identified mangroves as major estuarine sources for dissolved carbon (Bouillon et al., 2007; Ho et al., 2017; Ray et al., 2018b). Ho et al. (2017) estimated that at Shark River 65% of the estuarine DIC was mangrove-derived with the remainder

being carbonate dissolution, since Shark River drains a carbonate basin. Applying this ratio to the estuarine fluxes examined during this study, the mangrove derived DIC flux was ~8.3 x 10^5 mol/d while carbonate dissolution contributed ~4.5 x 10^5 mol/d.

In order to compare lateral export with literature values, fluxes were normalized to the inundated area. Since no high-resolution DEM was available for the study site, the inundated area is associated with large uncertainties, resulting in large uncertainty ranges for the scaled areal rates (Table 1). It has to be noted, that in the present study as well as in the literature, areal rates based on Eulerian approaches were higher than rates based on Lagrangian approaches. However, comparing similar methods, estuarine TAlk, DIC and DOC fluxes were consistent with previously published rates at Shark River as well as concordant with exchange rates reported for other mangrove-dominated systems (Table 3).

The Eulerian TAlk export (97 mmol/m^2/d) was slightly higher than the average TAlk export rate (76 mmol/m^2/d, n = 11) of mangrove-dominated sites examined with the Eulerian approach (Table 3). The slightly elevated TAlk export at Shark River compared to previous studies might be due to additional TAlk input by carbonate dissolution. The Lagrangian DIC export (80 mmol/m^2/d) was higher than values reported by Ho et al. (2017) (15 – 20 mmol/m^2/d). Comparing continuous DIC measurements from Ho et al. (2017) with data presented here suggests that larger estuarine DIC inputs during our study period were responsible for the higher DIC exports compared to Ho et al. (2017). The Eulerian DIC export (142 mmol/m^2/d) was close to the global DIC export (159 mmol/m^2/d) estimated by Bouillon et al. (2008), who suggested that DIC fluxes may be the unaccounted carbon sink in mangroves. Since this publication by Bouillon et al. (2008), a few studies quantified DIC exports from mangroves (149 ± 173 mmol/m^2/d, n = 15), with an average similar to the Eulerian export presented here (142 mmol/m^2/d).

The Eulerian DOC export (39 mmol/m^2/d) was very similar to values previously reported for Shark River (41 mmol/m^2/d) using a similar method (Bergamaschi et al., 2012), and marginally higher than the global average (34 mmol/m^2/d) (Bouillon et al., 2008). Lagrangian DOC export (12 mmol/m^2/d) was slightly higher than other Lagrangian export rates (2 mmol/m^2/d) at this site (Ho et al., 2017) and nearly identical to DOC export rates (13 mmol/m^2/d) analysed with flumes within the Shark River mangroves (Romigh et al., 2006).

The high agreement between observed TAlk, DIC and DOC export rates and other values reported in the literature using the same methodological approach, highlights the importance of the method choice. The method choice might have a higher impact on export rates than on differences between seasons, which appear to have little effect on DIC export rates in Shark River (Volta et al., 2018). Analysing fluxes at Gunboat Island (GI) for an entire year, Volta et al. (2018) found that DIC (23.2 - 25.4 ×10^5 mol/d) and CO_2 emissions (5.5 - 7.8 × 10^5 mol/d) varied little between seasons. Thus, even though this study was limited to a short period, the fluxes might still be representative for this site.

Shark River was a source of CO_2, CH_4 and N_2O to the atmosphere. The air-water flux of CO_2 (92 mmol/m^2/d) was close to previously measured emissions at this site (Ho et al., 2017), and was higher than the global average for mangrove systems (60 mmol/m^2/d) (Bouillon et al., 2008). High CO_2 emissions at Shark River are driven by upstream DIC input originating from freshwater marshes (Ho et al., 2017). In contrast to CO_2, CH_4 (60 µmol/m^2/d) and N_2O emissions (2 µmol/m^2/d) were much lower than the global average for mangroves (Murray et al., 2015; Rosentreter et al., 2018b). Air-water fluxes of CH_4 were possibly reduced by increased CH_4 oxidation within the water column as a result of oxygen rich fresh and saltwater input, compared to more oxygen limited waters such as tidal creeks.

571 Low N_2O emissions might be due to nitrate limitation within the mangrove area (Inglett et al.,
572 2011). Other pristine mangrove systems, which are naturally low in nitrogen, were found to
573 have minimal N_2O emissions (Reading et al., 2017) and even N_2O undersaturation (Maher et
574 al., 2016).

Table 3: Literature values for lateral dissolved carbon and alkalinity exchange (scaled to the inundated mangrove area) as well as greenhouse gas emissions.

Reference	Country	Site	TAlk exchange (mmol/m^2/d)	DIC exchange (mmol/m^2/d)	DOC exchange (mmol/m^2/d)	CO_2 exchange (mmol/m^2/d)	CH_4 exchange (µmol/m^2/d)	N_2O exchange (µmol/m^2/d)
This study	USA	Shark River	97 (48 - 193)[e] 64 (32 - 128)[l]	142 (71 - 284)[e] 80 (40 - 161)[l]	39 (20 - 79)[e] 12 (4 - 24)[l]	92	60	2
Ho et al. (2017) and Ho et al. (2014)	USA	Shark River (dry 1)		21 ± 12[l]	2 ± 1[l]	105 ± 9		
		Shark River (dry 2)		13 ± 14[l]	2 ± 4[l]	99 ± 6		
Bergamaschi et al. (2012)	USA	Shark River			41 ± 3[e]			
Romigh et al. (2006)	USA	Shark River			13[f]			
Maher et al. (2013a)	Australia	Moreton Bay (summer)		183[e]	41[e]			
		Moreton Bay (winter)		340[e]	12[e]			
Faber et al. (2014)	Australia	Western Port (WI)	310[e]	450[e]	25[e]	17		
		Western Port (CI)	46[e]	130[e]	0[e]	19		
Sippo et al. (2016) and Maher et al. (2016)	Australia	Darwin	116[e]	85[e]		40		- 0.1 ± 0.01
		Hinchinbrook Island	21[e]	22[e]		30		- 3 ± 0.06
		Seventeen Seventy	81[e]	-97[e]		10		- 2 ± 0.1
		Jacobs Well	12[e]	83[e]		19		- 3 ± 0.08
		Newcastle	116[e]	77[e]		46		0.7 ± 0.03
		Barwon Heads	-1[e]	-3[e]		9		- 1 ± 0.07
Sadat-Noori et al. (2016)	Australia	Korogoro Creek	23 ± 5[e c]	20 ± 4[e c]	9 ± 2[e c]	869	26000	
Maher et al. (2018)	Australia	Moreton Bay	96 ± 35[e]	212 ± 74[e]	59 ± 22[e]	23 – 42	33 – 54	
Santos et al. (2019)	Australia	Evans Head	12 ± 6[e c]	12 ± 6[e c]	2 ± 2[e c]	63 ± 166	270 ± 30	
Ray et al. (2018a)	India	Sundarbans		202[e]	162[e]			
Taillardat et al. (2018)	Vietnam	Can Gio		352 - 678[e]	21 - 68[e]	70 - 174		
Bouillon et al. (2008)	global			159 ± 120	34 ± 14	60 ± 45		
Rosentreter et al. (2018b)	global						288 ± 73	
Murray et al. (2015)	global							22 (2-144)

Note: Method: [e]Eulerian approach, [l]Lagrangian approach, [f]Flumes, [c]scaled to the catchment area

The Shark River estuary was a net source of TAlk and dissolved carbon to the coastal ocean and a source of greenhouse gases to the atmosphere (Figure 8). Most of the inorganic carbon was exported laterally (83 - 93%), mainly as DIC, whereas only a small share was emitted to the atmosphere as CO_2 and CH_4. Carbon burial rates (123 ± 19 g C/m^2/y) of the mangrove forest surrounding Shark River (Breithaupt et al., 2014) are two to four times lower than lateral DIC export (255 – 452 g C/m^2/y) presented here, emphasising the importance of considering lateral carbon export in blue carbon budgets. Upscaling all available TAlk and DIC export rates (Table 3) to the global mangrove area (Giri et al., 2011) suggests a global TAlk export of 4.8 Tmol/y and a DIC export of 146 Tg C/y, which is an order of magnitude higher than the global burial rate of ~26 Tg C/y estimated by Breithaupt et al. (2012). Both export rates are higher than previous global estimates for DIC (43 ± 12 Tg C/y) and TAlk (4.2 Tmol/y) export, which were limited to six Australian mangrove creeks (Sippo et al., 2016). However, the global estimates presented here are still based on a relatively small number of studies, and more research is clearly required to validate global export rates. This is especially the case in the low latitude tropics (0 – 5°) where most mangroves occur, but the number of estimates of TAlk and DIC export rates are very limited.

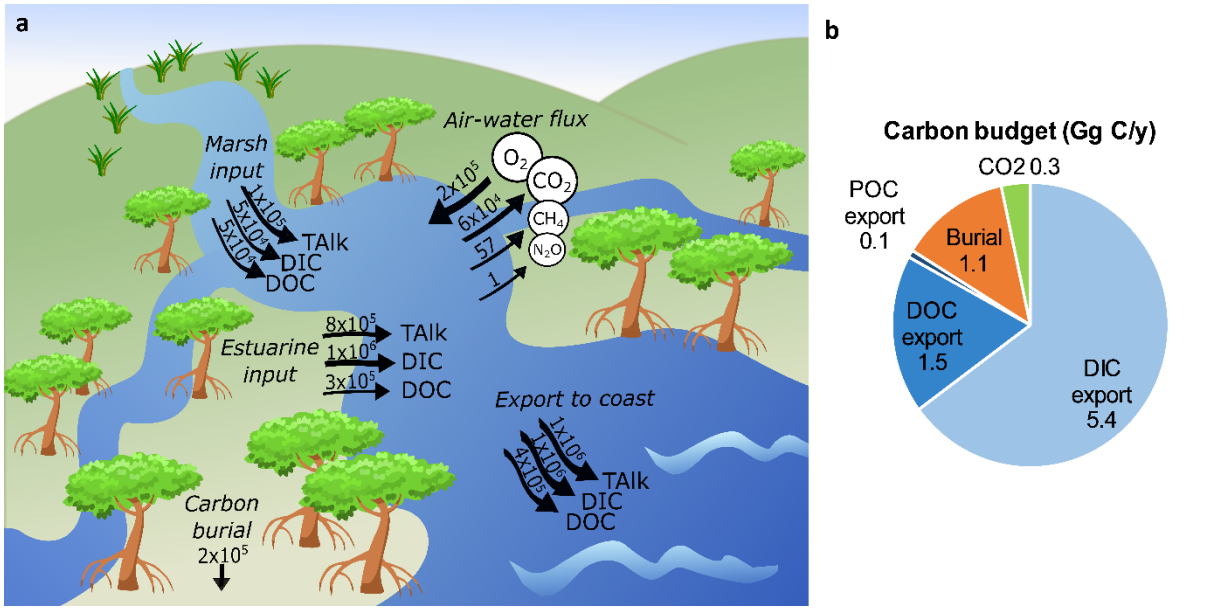

Figure 8. Alkalinity, dissolved carbon and greenhouse gas fluxes at the Shark River estuary are presented in mol/d (a). The estuarine carbon budget is presented in Gg C/y (b). Values for particulate organic carbon (POC) were retrieved from He et al. (2014), carbon burial from Breithaupt et al. (2014) and DIC, DOC and CO_2 fluxes were examined during the present study (b).

5 Conclusion

By combining spatial surveys and time series approaches at the mangrove-dominated Shark River, we found that the estuary was a source for alkalinity and dissolved carbon to the Gulf of Mexico, and a source of greenhouse gas emissions to the atmosphere. The dominant metabolic process changed along the estuary, from anaerobic processes in the upper estuary to a greater dominance of aerobic metabolism in the lower estuary. Additional to carbon remineralization, carbonate dissolution and porewater inputs were identified as important drivers controlling carbon fluxes. Lateral DIC export exceeds mangrove sedimentary carbon burial rates by at least twofold, resulting in an underestimation of the net carbon sequestration effect of mangroves. The majority of the exported DIC was carbonate alkalinity, which may buffer acidification of coastal waters. The climate change mitigation provided by the mangrove-dominated estuary was partly offset by CH_4 and N_2O emissions. However, greenhouse gas emissions were minor compared to carbon sequestration and alkalinity export. To accurately assess the capacity of OAlk to buffer coastal acidification, future studies should quantitatively account for OAlk in the TAlk pool, and characterise the organic compounds contributing to the OAlk pool. Furthermore, DOC and fDOM seem to be promising OAlk proxies, which may provide a less laborious option for quantifying OAlk. For researchers examining alkalinity, dissolved carbon and greenhouse gas dynamics in estuaries, it is recommended to combine both spatial and temporal approaches to provide independent estimates of fluxes and enhanced cross validation. We argue that accounting for lateral alkalinity and dissolved carbon export, as well as greenhouse gas fluxes, is crucial to evaluate the potential of mangroves to mitigate climate change. We therefore urge the scientific community to work towards integrating these processes into blue carbon budgets.

Literature

Atwood, T. B., R. M. Connolly, H. Almahasheer, P. E. Carnell, C. M. Duarte, C. J. E. Lewis, et al. (2017). Global patterns in mangrove soil carbon stocks and losses. *Nature Climate Change*, *7*(7), 523, doi:10.1038/NCLIMATE3326

Baker, A., and R. G. Spencer (2004). Characterization of dissolved organic matter from source to sea using fluorescence and absorbance spectroscopy. *Science of the Total Environment*, *333*(1-3), 217-232, doi:10.1016/j.scitotenv.2004.04.013

Barr, J. G., V. Engel, J. D. Fuentes, J. C. Zieman, T. L. O'Halloran, T. J. Smith III, and G. H. Anderson (2010). Controls on mangrove forest-atmosphere carbon dioxide exchanges in western Everglades National Park. *Journal of Geophysical Research*, *115*(G2), G02020, doi:10.1029/2009JG001186

Benson, B. B., and D. Krause (1984). The concentration and isotopic fractionation of oxygen dissolved in freshwater and seawater in equilibrium with the atmosphere. *Limnology and Oceanography*, *29*(3), 620-632, doi:10.4319/lo.1984.29.3.0620

Bergamaschi, B. A., D. P. Krabbenhoft, G. R. Aiken, E. Patino, D. G. Rumbold, and W. H. Orem (2012). Tidally driven export of dissolved organic carbon, total mercury, and methylmercury from a mangrove-dominated estuary. *Environmental Science & Technology*, *46*(3), 1371-1378, doi:10.1021/es2029137

Bouillon, S., A. V. Borges, E. Castañeda-Moya, K. Diele, T. Dittmar, N. C. Duke, et al. (2008). Mangrove production and carbon sinks: a revision of global budget estimates. *Global Biogeochemical Cycles*, *22*(2), GB2013, doi:10.1029/2007GB003052

Bouillon, S., F. Dehairs, B. Velimirov, G. Abril, and A. V. Borges (2007). Dynamics of organic and inorganic carbon across contiguous mangrove and seagrass systems (Gazi Bay, Kenya). *Journal of Geophysical Research*, *112*(G2), G02018, doi:10.1029/2006JG000325

Breithaupt, J. L., J. M. Smoak, T. J. Smith III, and C. J. Sanders (2014). Temporal variability of carbon and nutrient burial, sediment accretion, and mass accumulation over the past century in a carbonate platform mangrove forest of the Florida Everglades. *Journal of Geophysical Research: Biogeosciences*, *119*(10), 2032-2048, doi:10.1002/ 2014JG002715

Breithaupt, J. L., J. M. Smoak, T. J. Smith III, C. J. Sanders, and A. Hoare (2012). Organic carbon burial rates in mangrove sediments: Strengthening the global budget. *Global Biogeochemical Cycles*, *26*(3), GB3011, doi:10.1029/2012GB004375

Burdige, D. (2011). Estuarine and coastal sediments–coupled biogeochemical cycling. *Treatise on Estuarine and Coastal Science*, *5*, 279-308, doi:10.1002/2015GB005324

Burnett, W., G. Kim, and D. Lane-Smith (2001). A continuous monitor for assessment of ^{222}Rn in the coastal ocean. *Journal of Radioanalytical and Nuclear Chemistry*, *249*(1), 167-172, doi:10.1023/A:1013217821419

Cai, W.-J., Y. Wang, and R. E. Hodson (1998). Acid-base properties of dissolved organic matter in the estuarine waters of Georgia, USA. *Geochimica et Cosmochimica Acta*, *62*(3), 473-483, doi:10.1016/S0016-7037(97)00363-3

Call, M., D. T. Maher, I. R. Santos, S. Ruiz-Halpern, P. Mangion, C. J. Sanders, et al. (2015). Spatial and temporal variability of carbon dioxide and methane fluxes over semi-diurnal and spring–neap–spring timescales in a mangrove creek. *Geochimica et Cosmochimica Acta*, *150*, 211-225, doi:10.1016/j.gca.2014.11.023

Call, M., I. R. Santos, T. Dittmar, C. E. de Rezende, N. E. Asp, and D. T. Maher (2019). High pore-water derived CO_2 and CH_4 emissions from a macro-tidal mangrove creek in the Amazon region. *Geochimica et Cosmochimica Acta*, *247*, 106-120, doi:10.1016/j.gca.2018.12.029

Chen, R., and R. R. Twilley (1999). Patterns of mangrove forest structure and soil nutrient dynamics along the Shark River Estuary, Florida. *Estuaries*, *22*(4), 955-970, doi:10.2307/1353075

Chen, X., F. Zhang, Y. Lao, X. Wang, J. Du, and I. R. Santos (2018). Submarine groundwater discharge-derived carbon fluxes in mangroves: An important component of blue carbon budgets? *Journal of Geophysical Research: Oceans*, *123*(9), 6962-6979, doi:10.1029/2018JC014448

Dickson, A. G. (2010). Standards for ocean measurements. *Oceanography*, *23*(3), 34-47, doi:10.5670/oceanog.2010.22

Donato, D. C., J. B. Kauffman, D. Murdiyarso, S. Kurnianto, M. Stidham, and M. Kanninen (2011). Mangroves among the most carbon-rich forests in the tropics. *Nature geoscience*, *4*(5), 293, doi:10.1038/NGEO1123

Emerson, S., and J. Hedges (2008). Chemical oceanography and the marine carbon cycle. *Cambridge University Press*, doi:10.1017/CBO9780511793202

Faber, P. A., V. Evrard, R. J. Woodland, I. C. Cartwright, and P. L. Cook (2014). Pore-water exchange driven by tidal pumping causes alkalinity export in two intertidal inlets. *Limnology and Oceanography*, *59*(5), 1749-1763, doi:10.4319/lo.2014.59.5.1749

Fong, M. B., and A. G. Dickson (2019). Insights from GO-SHIP hydrography data into the thermodynamic consistency of CO_2 system measurements in seawater. *Marine Chemistry*, *211*, 52-63, doi:10.1016/j.marchem.2019.03.006

Friederich, G., P. Walz, M. Burczynski, and F. Chavez (2002). Inorganic carbon in the central California upwelling system during the 1997–1999 El Niño–La Niña event. *Progress in Oceanography*, *54*(1-4), 185-203, doi:10.1016/S0079-6611(02)00049-6.

Friesen, S. D., C. Dunn, and C. Freeman (2018). Decomposition as a regulator of carbon accretion in mangroves: a review. *Ecological Engineering*, *114*, 173-178, doi:10.1016/j.ecoleng.2017.06.069

Friis, K., A. Körtzinger, and D. W. Wallace (2003). The salinity normalization of marine inorganic carbon chemistry data. *Geophysical Research Letters*, *30*(2), 1085, doi:10.1029/2002GL015898

Giri, C., E. Ochieng, L. L. Tieszen, Z. Zhu, A. Singh, T. Loveland, et al. (2011). Status and distribution of mangrove forests of the world using earth observation satellite data. *Global Ecology and Biogeography*, *20*(1), 154-159, doi:10.1111/j.1466-8238.2010.00584.x

Gleeson, J., I. R. Santos, D. T. Maher, and L. Golsby-Smith (2013). Groundwater–surface water exchange in a mangrove tidal creek: evidence from natural geochemical tracers and implications for nutrient budgets. *Marine Chemistry*, *156*, 27-37, doi:10.1016/j.marchem.2013.02.001

Hammer, K., B. Schneider, K. Kuliński, and D. E. Schulz-Bull (2017). Acid-base properties of Baltic Sea dissolved organic matter. *Journal of Marine Systems*, *173*, 114-121, doi:10.1016/j.jmarsys.2017.04.007

He, D., R. N. Mead, L. Belicka, O. Pisani, and R. Jaffé (2014). Assessing source contributions to particulate organic matter in a subtropical estuary: A biomarker approach. *Organic Geochemistry*, *75*, 129-139, doi:10.1016/j.orggeochem.2014.06.012

Hernández-Ayon, M. J., A. Alberto, A. Dickson, T. Camiro-Vargas, and E. Valenzuela-Espinoza (2007). Estimating the contribution of organic bases from microalgae to the titration alkalinity in coastal seawaters. *Limnology and Oceanography: Methods*, *5*(7), 225-232, doi:10.4319/lom.2007.5.225

Ho, D. T., N. Coffineau, B. Hickman, N. Chow, T. Koffman, and P. Schlosser (2016). Influence of current velocity and wind speed on air-water gas exchange in a mangrove estuary. *Geophysical Research Letters*, *43*(8), 3813-3821, doi:10.1002/2016GL068727

Ho, D. T., S. Ferrón, V. C. Engel, W. T. Anderson, P. K. Swart, R. M. Price, and L. Barbero (2017). Dissolved carbon biogeochemistry and export in mangrove-dominated rivers of the Florida Everglades. *Biogeosciences*, *14*(9), 2543-2559, doi:10.5194/bg-14-2543-2017

Ho, D. T., S. Ferrón, V. C. Engel, L. G. Larsen, and J. G. Barr (2014). Air-water gas exchange and CO_2 flux in a mangrove-dominated estuary. *Geophysical Research Letters*, *41*(1), 108-113, doi:10.1002/2013GL058785

Hu, X. (2020). Effect of Organic Alkalinity on Seawater Buffer Capacity: A Numerical Exploration. *Aquatic Geochemistry*, doi:10.1007/s10498-020-09375-x

Hunt, C., J. Salisbury, and D. Vandemark (2011). Contribution of non-carbonate anions to total alkalinity and overestimation of pCO_2 in New England and New Brunswick rivers. *Biogeosciences*, *8*(10), 3069-3076, doi:10.5194/bg-8-3069-2011

Inglett, P., V. Rivera-Monroy, and J. Wozniak (2011). Biogeochemistry of nitrogen across the Everglades landscape. *Critical Reviews in Environmental Science and Technology*, *41*(S1), 187-216, doi:10.1080/10643389.2010.530933

IPCC (2014). *Climate change 2013: the physical science basis: Working Group I contribution to the Fifth assessment report of the Intergovernmental Panel on Climate Change*, Cambridge University Press.

Kaul, L. W., and P. N. Froelich (1984). Modeling estuarine nutrient geochemistry in a simple system. *Geochimica et Cosmochimica Acta*, *48*(7), 1417-1433, doi:10.1016/0016-7037(84)90399-5

Kim, H. C., and K. Lee (2009). Significant contribution of dissolved organic matter to seawater alkalinity. *Geophysical Research Letters*, *36*(20), L20603, doi:10.1029/2009GL040271

Ko, Y. H., K. Lee, K. H. Eom, and I. S. Han (2016). Organic alkalinity produced by phytoplankton and its effect on the computation of ocean carbon parameters. *Limnology and Oceanography*, *61*(4), 1462-1471, doi:10.1002/lno.10309

Koeve, W., and A. Oschlies (2012). Potential impact of DOM accumulation on fCO_2 and carbonate ion computations in ocean acidification experiments. *Biogeosciences*, *9*(10), 3787-3798, doi:10.5194/bg-9-3787-2012

Koné, Y.-M., and A. Borges (2008). Dissolved inorganic carbon dynamics in the waters surrounding forested mangroves of the Ca Mau Province (Vietnam). *Estuarine, Coastal and Shelf Science*, *77*(3), 409-421, doi:10.1016/j.ecss.2007.10.001

Kuliński, K., B. Schneider, K. Hammer, U. Machulik, and D. Schulz-Bull (2014). The influence of dissolved organic matter on the acid–base system of the Baltic Sea. *Journal of Marine Systems*, *132*, 106-115, doi:10.1016/j.jmarsys.2014.01.011

Lewis, E., and D. Wallace (1998). Program developed for CO_2 system calculations, carbon dioxide information analysis center. *Oak Ridge National Laboratory, US Department of Energy*, doi:10.2172/639712

Lukawska-Matuszewska, K., W. Grzybowski, A. Szewczun, and P. Tarasiewicz (2018). Constituents of organic alkalinity in pore water of marine sediments. *Marine Chemistry*, *200*, 22-32, doi:10.1016/j.marchem.2018.01.012

Maher, D. T., M. Call, I. R. Santos, and C. J. Sanders (2018). Beyond burial: Lateral exchange is a significant atmospheric carbon sink in mangrove forests. *Biology Letters*, *14*(7), 20180200, doi:10.1098/rsbl.2018.0200

Maher, D. T., and B. D. Eyre (2010). Benthic fluxes of dissolved organic carbon in three temperate Australian estuaries: Implications for global estimates of benthic DOC fluxes. *Journal of Geophysical Research: Biogeosciences*, *115*(G4), doi:10.1029/2010JG001433

Maher, D. T., and B. D. Eyre (2012). Carbon budgets for three autotrophic Australian estuaries: Implications for global estimates of the coastal air-water CO_2 flux. *Global Biogeochemical Cycles*, *26*(1), GB1032, doi:10.1029/2011GB004075

Maher, D. T., I. R. Santos, L. Golsby-Smith, J. Gleeson, and B. D. Eyre (2013a). Groundwater-derived dissolved inorganic and organic carbon exports from a mangrove tidal creek: The missing mangrove carbon sink? *Limnology and Oceanography*, *58*(2), 475-488, doi:10.4319/lo.2013.58.2.0475

Maher, D. T., I. R. Santos, J. R. Leuven, J. M. Oakes, D. V. Erler, M. C. Carvalho, and B. D. Eyre (2013b). Novel use of cavity ring-down spectroscopy to investigate aquatic carbon cycling from microbial to ecosystem scales. *Environmental Science & Technology*, *47*(22), 12938-12945, doi:10.1021/es4027776

Maher, D. T., J. Z. Sippo, D. R. Tait, C. Holloway, and I. R. Santos (2016). Pristine mangrove creek waters are a sink of nitrous oxide. *Scientific Reports*, *6*, 25701, doi:10.1038/srep25701

Martz, T. R., J. G. Connery, and K. S. Johnson (2010). Testing the Honeywell Durafet® for seawater pH applications. *Limnology and Oceanography: Methods*, *8*(5), 172-184, doi:10.4319/lom.2010.8.172

Millero, F. J. (2010). Carbonate constants for estuarine waters. *Marine and Freshwater Research*, *61*(2), 139-142, doi:10.1071/MF09254

Moran, M. A., W. M. Sheldon, and R. G. Zepp (2000). Carbon loss and optical property changes during long-term photochemical and biological degradation of estuarine dissolved organic matter. *Limnology and Oceanography*, *45*(6), 1254-1264, doi:10.4319/lo.2000.45.6.1254

Murray, R. H., D. V. Erler, and B. D. Eyre (2015). Nitrous oxide fluxes in estuarine environments: response to global change. *Global Change Biology*, *21*(9), 3219-3245, doi:10.1111/gcb.12923

Olmsted, I. C., and T. V. Armentano (1997). *Vegetation of Shark Slough, Everglades National Park*, South Florida Natural Resources Center, Everglades National Park Homestead, FL.

Petuch, E. J., and C. Roberts (2007). *The geology of the Everglades and adjacent areas*, CRC Press.

Pierrot, D., C. Neill, K. Sullivan, R. Castle, R. Wanninkhof, H. Lüger, et al. (2009). Recommendations for autonomous underway pCO_2 measuring systems and data-reduction routines. *Deep Sea Research Part II*, *56*(8-10), 512-522, doi:10.1016/j.dsr2.2008.12.005

Ray, R., A. Baum, T. Rixen, G. Gleixner, and T. Jana (2018a). Exportation of dissolved (inorganic and organic) and particulate carbon from mangroves and its implication to the carbon budget in the Indian Sundarbans. *Science of the Total Environment*, *621*, 535-547, doi:doi.org/10.1016/j.scitotenv.2017.11.225

Ray, R., E. Michaud, R. Aller, V. Vantrepotte, G. Gleixner, R. Walcker, et al. (2018b). The sources and distribution of carbon (DOC, POC, DIC) in a mangrove dominated estuary (French Guiana, South America). *Biogeochemistry*, *138*(3), 297-321, doi:10.1007/s10533-018-0447-9

Reading, M. J., I. R. Santos, D. T. Maher, L. C. Jeffrey, and D. R. Tait (2017). Shifting nitrous oxide source/sink behaviour in a subtropical estuary revealed by automated time series observations. *Estuarine, Coastal and Shelf Science*, *194*, 66-76, doi:10.1016/j.ecss.2017.05.017

Romigh, M. M., S. E. Davis, V. H. Rivera-Monroy, and R. R. Twilley (2006). Flux of organic carbon in a riverine mangrove wetland in the Florida Coastal Everglades. *Hydrobiologia*, *569*(1), 505-516, doi:10.1007/s10750-006-0152-x

Rosentreter, J. A., D. Maher, D. Erler, R. Murray, and B. Eyre (2018a). Seasonal and temporal CO_2 dynamics in three tropical mangrove creeks–A revision of global mangrove CO_2 emissions. *Geochimica et Cosmochimica Acta*, *222*, 729-745, doi:10.1016/j.gca.2017.11.026

Rosentreter, J. A., D. T. Maher, D. V. Erler, R. H. Murray, and B. D. Eyre (2018b). Methane emissions partially offset "blue carbon" burial in mangroves. *Science Advances*, *4*(6), eaao4985, doi:10.1126/sciadv.aao4985

Sadat-Noori, M., D. T. Maher, and I. R. Santos (2016). Groundwater discharge as a source of dissolved carbon and greenhouse gases in a subtropical estuary. *Estuaries and Coasts*, *39*(3), 639-656, doi:10.1007/s12237-015-0042-4

Santos, I. R., D. T. Maher, and B. D. Eyre (2012). Coupling automated radon and carbon dioxide measurements in coastal waters. *Environmental Science & Technology*, *46*(14), 7685-7691, doi:10.1021/es301961b

Santos, I. R., D. T. Maher, R. Larkin, J. R. Webb, and C. J. Sanders (2019). Carbon outwelling and outgassing vs. burial in an estuarine tidal creek surrounded by mangrove and saltmarsh wetlands. *Limnology and Oceanography*, *64*(3), 996-1013, doi:10.1002/lno.11090

Sholkovitz, E., E. Boyle, and N. Price (1978). The removal of dissolved humic acids and iron during estuarine mixing. *Earth and Planetary Science Letters*, *40*(1), 130-136, doi:10.1016/0012-821X(78)90082-1

Sippo, J. Z., D. T. Maher, D. R. Tait, C. Holloway, and I. R. Santos (2016). Are mangroves drivers or buffers of coastal acidification? Insights from alkalinity and dissolved inorganic carbon export estimates across a latitudinal transect. *Global Biogeochemical Cycles*, *30*(5), 753-766, doi:10.1002/2015gb005324

Stieglitz, T. C., J. F. Clark, and G. J. Hancock (2013). The mangrove pump: the tidal flushing of animal burrows in a tropical mangrove forest determined from radionuclide budgets. *Geochimica et Cosmochimica Acta*, *102*, 12-22, doi:10.1016/j.gca.2012.10.033

Suryaputra, I. G., I. R. Santos, M. Huettel, W. Burnett, and T. Dittmar (2015). Non-conservative behavior of fluorescent dissolved organic matter (FDOM) within a subterranean estuary. *Continental Shelf Research*, *110*, 183-190, doi:10.1016/j.csr.2015.10.011

Taillardat, P., P. Willemsen, C. Marchand, D. Friess, D. Widory, P. Baudron, et al. (2018). Assessing the contribution of porewater discharge in carbon export and CO_2 evasion in a mangrove tidal creek (Can Gio, Vietnam). *Journal of Hydrology*, *563*, 303–318, doi:10.1016/j.jhydrol.2018.05.042

Tait, D. R., D. T. Maher, P. A. Macklin, and I. R. Santos (2016). Mangrove pore water exchange across a latitudinal gradient. *Geophysical Research Letters*, *43*(7), 3334-3341, doi:10.1002/ 2016GL068289

Tishchenko, P. Y., K. Wallmann, N. Vasilevskaya, T. Volkova, V. Zvalinskii, N. Khodorenko, and E. Shkirnikova (2006). The contribution of organic matter to the alkaline reserve of natural waters. *Oceanology*, *46*(2), 192-199, doi:10.1134/S0001437006020068

U.S. Geological Survey (2018), National Water Information System data available on the World Wide Web (USGS Water Data for the Nation), accessed 13 August 2019, at URL: https://waterdata.usgs.gov/nwis/uv, edited.

Ulfsbo, A., K. Kuliński, L. G. Anderson, and D. R. Turner (2015). Modelling organic alkalinity in the Baltic Sea using a Humic-Pitzer approach. *Marine Chemistry*, *168*, 18-26, doi:10.1016/j.marchem.2014.10.013

Volta, C., D. T. Ho, G. Friederich, V. C. Engel, and M. Bhat (2018). Influence of water management and natural variability on dissolved inorganic carbon dynamics in a mangrove-dominated estuary. *Science of the Total Environment*, *635*, 479-486, doi:10.1016/j.scitotenv.2018.04.088

Wanninkhof, R. (2014). Relationship between wind speed and gas exchange over the ocean revisited. *Limnology and Oceanography: Methods*, *12*(6), 351-362, doi:10.4319/lom.2014.12.351

Webb, J. R., D. T. Maher, and I. R. Santos (2016). Automated, in situ measurements of dissolved CO_{-2}, CH_4, and $\delta^{13}C$ values using cavity enhanced laser absorption spectrometry: Comparing response times of air-water equilibrators. *Limnology and Oceanography: Methods*, *14*(5), 323-337, doi:10.1002/lom3.10092

Weiss, R., and B. Price (1980). Nitrous oxide solubility in water and seawater. *Marine Chemistry*, *8*(4), 347-359, doi:10.1016/0304-4203(80)90024-9

Weiss, R. F. (1974). Carbon dioxide in water and seawater: the solubility of a non-ideal gas. *Marine Chemistry*, *2*(3), 203-215, doi:10.1016/0304-4203(74)90015-2

Wiesenburg, D. A., and N. L. Guinasso Jr (1979). Equilibrium solubilities of methane, carbon monoxide, and hydrogen in water and sea water. *Journal of Chemical and Engineering Data*, *24*(4), 356-360, doi:10.1021/je60083a006

Yang, B., R. H. Byrne, and M. Lindemuth (2015). Contributions of organic alkalinity to total alkalinity in coastal waters: A spectrophotometric approach. *Marine Chemistry*, *176*, 199-207, doi:10.1016/j.marchem.2015.09.008

Zablocki, J. A., A. J. Andersson, and N. R. Bates (2011). Diel aquatic CO_2 system dynamics of a Bermudian mangrove environment. *Aquatic Geochemistry*, *17*(6), 841, doi:10.1007/s10498-011-9142-3

Acknowledgments, Samples, and Data

This research project was funded by the Australian Research Council (DP180101285) and the National Aeronautics and Space Administration (NNX14AJ92G) under the Carbon Cycle Program. We are particularly grateful to Benjamin Hickman for the technical support during the fieldtrip and the data analysis. We also like to thank James Ash for supporting us in the field, as well as Matheus Carvalho de Carvalho for conducting the DOC measurements. The authors declare that there is no conflict of interest. Datasets for this research are available on the PANGAEA database (https://issues.pangaea.de/browse/PDI-23888).